Palaeogeography, Palaeoclimatology, Palaeoecology 446 (2016) 326–337

Contents lists available at ScienceDirect

Palaeogeography, Palaeoclimatology, Palaeoecology

journal homepage: www.elsevier.com/locate/palaeo

Global distribution of Köppen–Geiger climate types during the Last Glacial Maximum, Mid-Holocene, and present

Jinwoong Yoo [a,1], Robert V. Rohli [b]

[a] Department of Earth and Planetary Sciences, University of New Mexico, Albuquerque, NM 87131, USA
[b] Department of Geography and Anthropology, Louisiana State University, Baton Rouge, LA 70803-4105, USA

ARTICLE INFO

Article history:
Received 27 August 2015
Received in revised form 12 December 2015
Accepted 14 December 2015
Available online 20 December 2015

Keywords:
Köppen–Geiger climate type
Last Glacial Maximum
Mid-Holocene
Paleoclimate
Climate change

ABSTRACT

This research presents Köppen–Geiger (K-G) climate type maps of the Last Glacial Maximum (LGM) of 21,000 years ago (21 ka), the mid-Holocene (MH) of 6 ka, and the present (1976–2005). Data used to calculate and map the K-G climate type are-year monthly mean 2-m air temperature and precipitation from the National Center for Atmospheric Research (NCAR) Community Climate System Model version 4 (CCSM4)—Community Atmosphere Model version 4 (CAM4) as part of the Coupled Model Intercomparison Project Phase 5 (CMIP5). Results suggest that the model depicts similar modern climate distributions as in data-based research, excepting a larger distribution of tropical wet–dry and humid subtropical types, and a smaller distribution of hot arid and hot semi-arid types. The modeled modern K-G climate types cover similar percentages of Earth's terrestrial and marine surface as during the MH, with slight enlargement of the tropical wet–dry and decreased area of mesothermal monsoonal hot summer type in the modern period. At the LGM, the K-G Polar (E) climate was far more extensive than in modern times, with concurrent decreases in area of the Tropical (A) climates. Because Köppen-type classifications are intended to mimic the biome distributions, these results may be helpful in identifying biotic realms from the geologic past and the potential vegetative response to future climate changes.

1. Introduction

As the manifestations and impacts of global climate changes both due to anthropogenic activity and natural variability have received increased attention in recent years, it is recognized that paleoclimate research can be useful for evaluating the models used for future climate projections by comparison to Earth's recent past (Harrison et al., 2014). The Last Glacial Maximum (LGM) 21,000 years ago (21 ka) and the mid-Holocene (MH) of 6 ka were characterized by contrasting climate forcing compared to the current climate (Braconnot et al., 2012). Since the height of the LGM, when CO_2 and CH_4 mixing ratios were perhaps 185 ppm and 350 ppb, respectively (Korty et al., 2012a; Otto-Bliesner et al., 2006), the Earth has warmed substantially. The warming is attributable to the collective effects of the phase of cyclical components of Earth's orbital and axial oscillations (i.e., Milankovitch cycles) that promote warming, increasing greenhouse gas concentrations (both natural and anthropogenic), and changing boundary conditions triggered by positive feedbacks such as Earth–albedo–ice (Otto-Bliesner et al., 2006). Current "best guess" estimates from proxy and modeling data suggest that at the LGM, surface temperatures were perhaps 2 °C below today's values in the tropics (Broccoli, 2000) and perhaps 30 °C colder than today over what was then the Laurentide Ice Sheet (Braconnot et al., 2007; Korty et al., 2012a). Otto-Bliesner et al. (2006) estimate that after 15,000 years of warming, the MH was characterized by CO_2 and NO mixing ratios of about 280 ppm and 270 ppb, respectively – similar to those of the 1700s – with slightly decreased CH_4 mixing ratios as compared to the immediate preindustrial era (650 vs. 760 ppb).

One interesting difference between the Sun–Earth geometry of the MH and that today is that perihelion during the MH occurred during September, while today's perihelion is in January (Korty et al., 2012b). The September perihelion would have allowed for relatively uniformly increased top-of-atmosphere solar radiation flux densities across the northern hemisphere (but likely decreases for the southern hemisphere) compared to today. By contrast, today's January perihelion provides little (substantial) additional solar radiation for the northern (southern) hemisphere high latitudes, which lie in near-continuous darkness (daylight) at that time of year. Thus, the comparative analysis of global climate patterns from the LGM to the MH to modern times can provide a clearer picture of the Earth's climate response to the change in influence of the Earth–Sun axial and orbital geometry and greenhouse and ice–albedo forcing.

The spatial variation of climate types, such as those identified by Köppen (1884, 1936, 2011), between the LGM, MH, and modern period can address the question of the extent to which the climate system's

E-mail address: jinwoong.yoo@gmail.com (J. Yoo).
[1] Tel.: +1 505 990 7198; fax: +1 505 277 8843.

http://dx.doi.org/10.1016/j.palaeo.2015.12.010
0031-0182/

response to the changing inputs was uniform globally. Recent availability of spatially comprehensive long-term datasets from general circulation model (GCM) simulations has made possible the global display of the spatial extent of climate types through time. As part of the effort to better understand the twenty-first century climate by reducing uncertainties from various model grid settings, the Paleoclimate Modeling Intercomparison Project (PMIP) simulates past climates using the same models used for future projections (Braconnot et al., 2012). The PMIP Phase III (PMIP3)/CMIP5 includes simulations of the LGM and MH as well as the current climate, allowing for some of the outstanding scientific questions posed in the Intergovernmental Panel on Climate Change Fourth Assessment Report (IPCC AR4; Brady et al., 2013) to be addressed. The purpose of this research is to derive estimates of the geography and extent of the Köppen-type classification with modification proposed by Geiger (K-G; Geiger, 1961) at the time of the LGM of approximately 21 ka BP and the MH (6 ka) and to compare the geography and extent of those climate types to those of the same climate types in the present, over both terrestrial and marine surfaces.

2. Overview of Köppen-type classification studies

Kottek et al. (2006) and Peel et al. (2007) were among the first to provide a terrestrial world map of a Köppen-type classification using a digitally gridded dataset; both studies selected the modification proposed by Geiger (1961). Zhang and Yan (2014) derived climate categories on the terrestrial Earth using K-means cluster analysis (Forgy, 1965) and found that these objectively determined categories coincide well with mapped Köppen–Geiger (K-G) types. The National Centers for Environmental Prediction/National Center for Atmospheric Research (NCEP/NCAR) Reanalysis dataset (Kalnay et al., 1996) has been employed in other updated global climate classifications, including for climate types over the oceans (Rohli et al., 2015a).

Beck et al. (2006) and Rubel and Kottek (2010) developed a series of world maps of the Köppen-based climate types over various time intervals in the twentieth century as a means of displaying temporal changes in the geographical position and area of climates. Not surprisingly, the results reflect the twentieth century's observed warming. Wong et al. (2012) identified relationships between trends in heat-related human comfort and stress indices and K-G-related shifts over subperiods of the twentieth century. Interestingly, however, Zhang and Yan (2014) found no distinct changes in the distribution of climate types between the four 25-year periods within the twentieth century using Cohen's (1960) kappa coefficient. Kalvová et al. (2003) were among the first to investigate the effectiveness of GCMs in reproducing observed climate types; Shin et al. (2012) noted that modeled output from 22 coupled GCMs has limited success in capturing twentieth century expansion of K-G arid types (particularly the steppe climates).

Temporal changes in the closely related Köppen–Trewartha (K-T) classification (Trewartha, 1968) during the period of record have also been analyzed recently by several researchers (e.g., Belda et al., 2014; Feng et al., 2011; Fraedrich et al., 2001; Kim et al., 2008). While both Köppen-based systems include one broad category (B) for arid climates, the aridity index differs slightly between the K-G and K-T approaches. Another major difference between the K-G and K-T classifications is that the former includes tropical (A), mesothermal (C), microthermal (D), and polar (E) climates, while in the latter, an additional broad category of climate types for boreal climates (E) is included, with temperature adjustments for A, C (which Trewartha (1968) labeled "subtropical"), D (temperate), and F (polar) types. A few recent studies have produced global dataset-based climate classifications using other systems, such as derivatives of Thornthwaite's (1948) original water-balance-based climate classification (e.g., Dantas et al., 2007; Elguindi et al., 2014; Feddema, 2005), Holdridge's (1947) Life Zones classification (e.g., Monserud and Leemans, 1992), and De Martonne's zones (Rahimi et al., 2013).

Other studies have used GCM simulations to compare the global extent of present-day K-G climate types to those under future global change scenarios. Using output from four GCMs, Kalvová et al. (2003) predicted that A and B climates would increase at the expense of D and E climates over the continental Earth by 2050. Feng et al. (2011) found that simulations made by 16 fully coupled models collectively suggest steady shrinking of polar and subarctic continental climate types and expansion of temperate and boreal oceanic climates through 2099. Hanf et al. (2012) concurred with that finding by using seven atmosphere–ocean coupled GCMs which also collectively suggested that drier A and B climates will prevail in the tropics and subtropics. Such changes could decrease crop yields in tropical, subtropical, and temperate climates (Berg et al., 2013). Mahlstein et al. (2013) suggested that the pace of shifting climate zones is likely to increase approximately linearly with increasing global temperature. K-T types have also been examined using such GCM simulations. For example, Feng et al. (2014) predicted that 31–46% of the terrestrial Earth will have a different climate type than at present by century's end.

Some researchers (e.g., Jacob et al., 2012) have successfully employed regional climate models (RCMs) for dynamic downscaling of GCM output for enhanced mapping of future K-T types, with validation by comparison to observed data. For example, an ensemble of 15 regional climate model simulations nested within six GCMs allowed Gallardo et al. (2013) to forecast that 22.3% of the grid points in a European study domain will have a different climate type by the 2021–2050 averaging period, with 48.1% changing their type by 2061–2090. In a similar methodology but across multiple regional domains, Teichmann et al. (2013) found that for the period 2006–2100, the RCMs forecasted slightly less warming effects in some regions in terms of climate types but with increases in aridity, as compared to the GCM projections.

Similar observational and projection-based analyses have been conducted at the regional scale, either for analyzing historical fluctuations in a K-G climate boundary (e.g., Mitchell and Kienholz, 1997; Suckling and Mitchell, 2000), a climate type such as the K-T polar tundra (ET) climate type (Wang and Overland, 2004) or K-G alpine tundra of the Rocky Mountain cordillera (Diaz and Eischeid, 2007), or some combination of these. Roderfeld et al. (2008) showed the poleward retreat in the K-G ET type and expansion of temperate climates in Scandinavia and northwestern Russia. Park et al. (2013) found increasing extent of K-T subtropical climate zones and reduction in D types by 2100 in the Republic of Korea, largely confirming the results of Yun et al. (2012) who employed both the K-T and K-G systems. Increasing areas of tropical and arid K-G types have also been projected across China (Baker et al., 2010), much of Asia (Shin and Bae, 2013), Australia (Crosbie et al., 2012), western Africa (Born et al., 2008), and Europe (Jylhä et al., 2010) by the end of the present century. Feng et al. (2011) projected large decreases in K-T-based polar and subarctic continental types by century's end, with different rates of change regionally.

One gap in the scholarly literature regarding shifts in Köppen and related climate types involves the comparison of the extent of types in the geological past to those of the present and the future under global change scenarios. This is unfortunate, because analogs of climate are often useful for providing the public with tangible descriptions of the changes. The extent of past K-G types has been estimated based on proxy evidence from high-latitude plant fossil assemblages during the mid-Miocene global cooling (Denk et al., 2013) and in China during the Eocene epoch (Zhang et al., 2012), but there is a general dearth of model-simulated paleo-reconstructions of Köppen types.

One notable exception is the work of Guetter and Kutzbach (1990) in the Cooperative Holocene Mapping Project (COHMAP; Kutzbach, 1988), who used an atmosphere–ocean GCM to estimate that 45% of the terrestrial Earth had a different climate type at the LGM of approximately 18 ka BP. Guetter and Kutzbach (1990) modified the numerical algorithm used by K-G to improve the correspondence between climate

type and biome type, but the method and categories were more reminiscent of K-G than K-T. Crucifix et al. (2005) refined the idea developed by Guetter and Kutzbach (1990) and focused on simulating vegetation distributions rather than climate types based on vegetation distributions during the LGM. Guetter and Kutzbach's (1990) work was pioneering, but the significant improvement in model performance and spatial resolution of modeled output of today call for a re-examination of the topic.

3. Materials and methods

Mapping of K-G climate types was done using the Community Climate System Model version 4 (CCSM4) simulation results for the LGM, MH, and modern periods as part of PMIP3/CMIP5. Those data were obtained from the NCAR Yellowstone supercomputer data storage. The CCSM4 GCM consists of four major components – for the atmosphere, ocean, land, and sea ice – integrated via a coupler (Gent et al., 2011). With a uniform resolution of 1.25° latitude by 0.9° longitude with 26 vertical layers, the Community Atmosphere Model (version 4; CAM4; Neale et al., 2013) was selected for the atmospheric component of the CCSM4. The land model uses version 4 of the Community Land Model (CLM4; Lawrence et al., 2012) with the same horizontal resolution as in CAM4. Despite the fixed plant functional type distribution at preindustrial values (Lawrence and Chase, 2007), the carbon–nitrogen biogeochemistry component of CLM4 can represent the change of the seasonal and interannual vegetation phenology which is responsive to

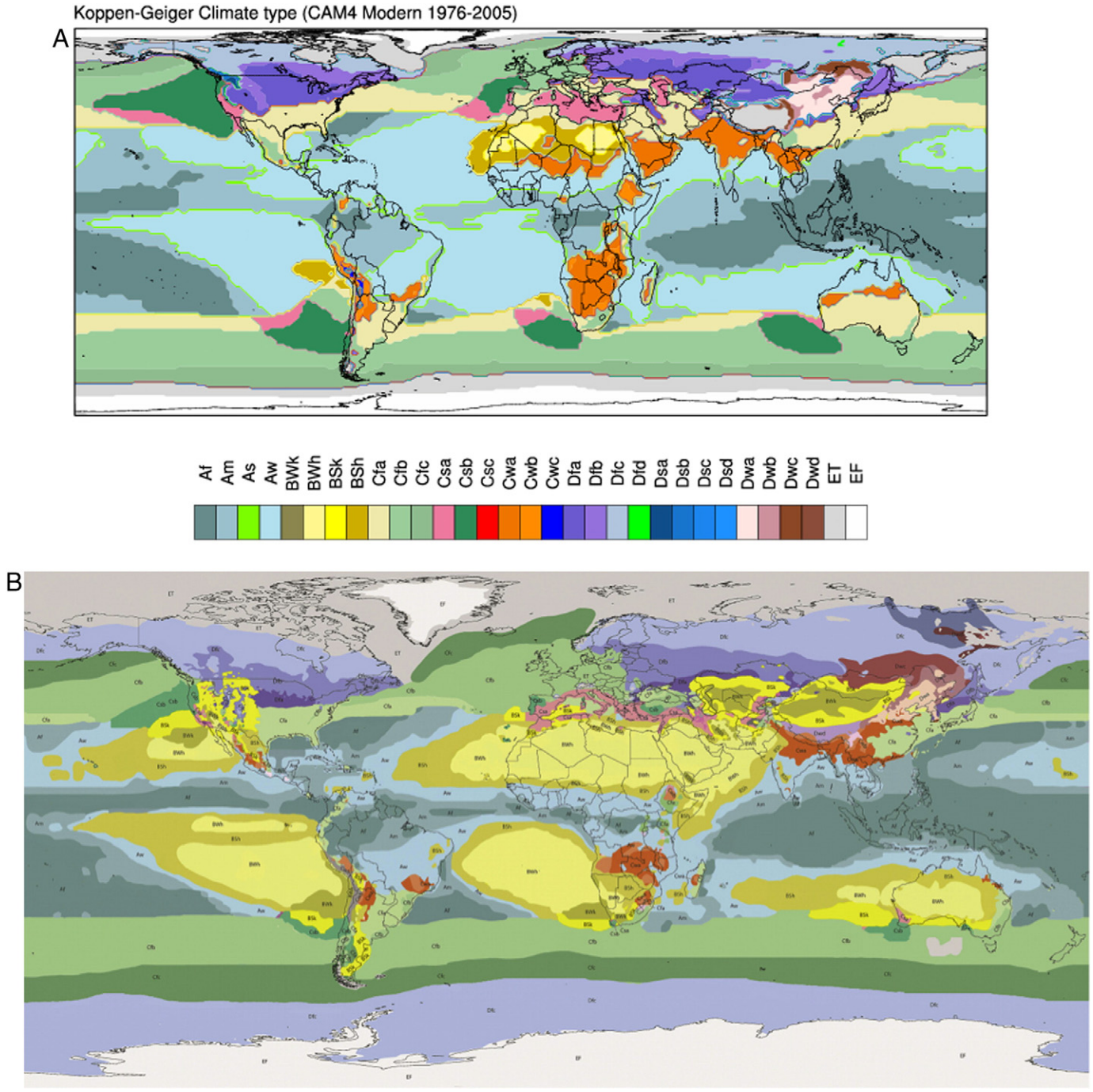

Fig. 1. K-G global climatic types. a) CCSM4-simulated values based on 1976–2005 data; b) values based on NCAR/NCEP reanalysis data for 1981–2010, from Rohli et al. (2015a)—reprinted with permission by McGraw-Hill.

the changed climate: the total leaf and stem area indices and vegetation canopy height (Brady et al., 2013; Thornton et al., 2007). The ocean model of the CCSM4 is the NCAR implementation of the Parallel Ocean Program version 2 (POP2) (http://www.cesm.ucar.edu/models/ccsm4.0/pop/). The sea ice model in the CCSM4 is a dynamical–thermodynamic formulation, which calculates most importantly a subgrid-scale ice thickness distribution and elastic–viscous–plastic rheology (Briegleb et al., 2004). The horizontal grid of POP2 and sea ice model is 320 × 384 points in which poles are located in Greenland and Antarctica (Brady et al., 2013). For more details on the CCSM4 model configuration, see Brady et al. (2013).

This study utilizes the same K-G criteria as used and described in detail by Rohli et al. (2015a). This procedure facilitates comparison of the extent of climate types to Rohli et al. (2015a) on the current climate types over land and ocean, to GCM-based simulations of future extent by Rubel and Kottek (2010), and at least in a qualitative sense, to the coarse grid cells produced in an early modeling study by Guetter and Kutzbach (1990). In the present study, 30-year mean 2-m air temperature and precipitation during the present state (1976–2005), the MH (6 ka), and the LGM (21 ka) from the CMIP5 simulations were used. Results retrieved from the CMIP5 CCSM4 (CAM4) data set are plotted in NCAR Command Language (NCL). As in Rohli et al. (2015a), the K-G climate types are shown both over land and ocean.

4. Results

4.1. Modern

Simulation of modern (i.e., 1976–2005) K-G climate types by CCSM4 CAM4 yields global terrestrial extents (Fig. 1a) that are similar to those of the corresponding types derived from Rohli et al. (2015a; Fig. 1b) and Rubel and Kottek (2010); Table 1). Nevertheless, some notable differences between the maps do exist, with the differences quantified in Table 2. For the total global area, the present analysis suggests that the tropical wet–dry (Aw) climate appears much more extensively (Table 2) and is the world's most widespread climate (Table 1), while Rohli et al. (2015a) only found Aw to rank third in total global extent. The humid subtropical (Cfa) type also appears more prominently here than in Rohli et al. (2015a). Conversely, the hot desert (BWh), hot semi-arid (BSh), and subpolar cool summer (Dfc) types appear less extensively than in Rohli et al. (2015a). It is possible that the lack of inclusion of the most recent hot years in the present dataset may partially explain the differences.

For the terrestrial-only analysis, the present analysis calculates Cfa as the most extensive type, while the other two studies ranked that type eighth and tenth (Table 1). By contrast, BWh is far less extensive in the present study, while the other studies ranked BWh as the most extensive type (Table 1). The second, third, and fourth most extensive types (Aw, Dfc, and ice cap (EF), respectively) are the same for all three studies. For the marine-only analysis, the largest differences are for Aw, which appears more extensively in the present study (as the world's most widespread climate type over the oceans; Table 1), and for Dfc, BSh, and BWh, which are less widespread over the oceans in the present study as compared to Rohli et al. (2015a; Table 2).

It is possible that errors in the modeled results and/or differences in the study period of analysis could account for some of these differences. The CCSM4 includes the climatologically cold years of the late 1970s in lieu of the globally hot years of 2006–2010, while Rohli et al. (2015a) excludes the late 1970s and includes years through 2010. The rapid contraction in ET and expansion of B climate types through the early 21st century have been noted previously (Chen and Chen, 2013). Differences may also be attributable to smoothing in the Rohli et al. (2015a) map due to their use of a relatively coarse (2.5 × 2.5-degree grid) spatial resolution of the National Centers for Environmental Prediction/NCAR Reanalysis dataset (Kalnay et al., 1996) and to differences in the interpolated datasets themselves. Finally, GCMs can exhibit large bias,

Table 1
Percentage of global, terrestrial, and marine surface area covered by each K-G climatic type: CCSM4 vs. existing literature.

	CCSM4 CAM4			Source: Rohli et al. (2015a)			Source: Rubel and Kottek (2010)
	1976–2005 (total Earth)	1976–2005 (terrestrial)	1976–2005 (marine)	1981–2010 (total Earth)	1981–2010 (terrestrial)	1981–2010 (marine)	1976–2000 (terrestrial)
Af	9.61	3.97	12.35	13.08	5.15	16.12	5.14
Am	12.18	8.24	14.09	7.77	2.55	9.77	3.50
As	—	—	—	—	—	—	0.60
Aw	19.94	12.21	23.70	9.76	10.77	9.37	11.08
BSh	1.35	2.65	0.72	8.01	5.79	8.86	6.07
BSk	—	—	—	2.53	5.61	1.36	4.88
BWh	0.41	1.22	0.02	9.47	13.06	8.1	13.45
BWk	—	—	—	1.43	2.93	0.85	3.07
Cfa	8.46	12.32	6.58	2.70	5.20	1.74	4.78
Cfb	10.80	4.46	13.88	12.34	3.75	15.63	3.32
Cfc	5.06	0.32	7.36	5.89	0.20	8.07	0.27
Csa	1.72	1.61	1.78	1.04	3.02	0.29	1.73
Csb	3.57	0.57	5.02	0.85	0.75	0.89	1.04
Csc	—	—	—	—	—	—	
Cwa	2.66	8.10	0.02	1.2	4.22	0.04	2.81
Cwb	0.51	1.55	—	0.58	1.63	0.18	1.08
Cwc	0.05	0.17	—	0.2	0.71	< 0.01	0.03
Dfa	2.29	6.96	0.03	0.48	1.45	0.1	0.98
Dfb	1.78	5.09	0.17	1.97	6.23	0.34	5.52
Dfc	3.79	10.90	0.33	9.27	10.02	8.99	9.66
Dfd	0.01	0.04	—	0.23	0.81	0.01	0.86
Dsa	0.05	0.14	—	< 0.01	0.01	< 0.01	0.14
Dsb	0.05	0.15	—	—	—	—	0.32
Dsc	0.01	0.04	—	—	—	—	0.77
Dsd	—	—	—	—	—	—	
Dwa	0.54	1.62	0.01	—	—	—	0.45
Dwb	0.28	0.86	—	0.25	0.87	0.01	0.90
Dwc	0.32	0.97	—	0.41	1.49	< 0.01	1.80
Dwd	—	—	—	0.05	0.17	0.01	0.17
ET	6.82	5.48	7.47	6.21	4.24	6.97	5.94
EF	7.74	10.34	6.48	4.26	9.40	2.30	9.56

Table 2
Differences in percentage of global, terrestrial, and marine surface area of modern K-G climatic types as calculated by CMIP5 Model (1976–2005) vs. Rohli et al. (2015a).

	CMIP5 Modern – Rohli et al. (2015a)		
	Total	Terrestrial	Marine
Af	−3.47	−1.18	−3.77
Am	4.41	5.69	4.32
As	0	0	0
Aw	10.18	1.44	14.33
BSh	−6.66	−3.14	−8.14
BSk	−2.53	−5.61	−1.36
BWh	−9.06	−11.84	−8.08
BWk	−1.43	−2.93	−0.85
Cfa	5.76	7.12	4.84
Cfb	−1.54	0.71	−1.75
Cfc	−0.83	0.12	−0.71
Csa	0.68	−1.41	1.49
Csb	2.72	−0.18	4.13
Csc	–	–	–
Cwa	1.46	3.88	−0.02
Cwb	−0.07	−0.08	−0.18
Cwc	−0.15	−0.54	–
Dfa	1.81	5.51	−0.07
Dfb	−0.19	−1.14	−0.17
Dfc	−5.48	0.88	−8.66
Dfd	−0.22	−0.77	−0.01
Dsa	0.05	0.13	–
Dsb	0.05	0.15	–
Dsc	0.01	0.04	–
Dsd	–	–	–
Dwa	0.54	1.62	0.01
Dwb	0.03	−0.01	−0.01
Dwc	−0.09	−0.52	–
Dwd	−0.05	−0.17	−0.01
ET	0.61	1.24	0.5
EF	3.48	0.94	4.18

Table 3
CMIP5-simulated percentage of earth's surface area covered by each K-G climatic type: Mid-Holocene compared to modern (1976–2005).

	Percentage of Global Surface Area During Mid-Holocene			Mid-Holocene Area—Modern Area		
	(Total)	(Terrestrial)	(Marine)	(Total)	(Terrestrial)	(Marine)
Af	8.42	3.65	10.73	−1.19	−0.32	−1.61
Am	11.98	8.07	13.88	−0.20	−0.18	−0.21
As	0.00	0.00	0.00	0.00	0.00	0.00
Aw	18.67	9.61	23.07	−1.27	−2.60	−0.63
BSh	0.75	1.24	0.51	−0.60	−1.41	−0.21
BSk	0.00	0.01	0.00	0.00	0.01	0.00
BWh	0.00	0.00	0.00	−0.41	−1.22	−0.02
BWk	0.00	0.00	0.00	0.00	0.00	0.00
Cfa	7.79	10.98	6.25	−0.67	−1.35	−0.34
Cfb	10.75	4.28	13.90	−0.05	−0.18	0.01
Cfc	5.22	0.26	7.64	0.17	−0.06	0.28
Csa	1.68	1.31	1.86	−0.04	−0.29	0.08
Csb	4.38	0.52	6.25	0.81	−0.05	1.23
Csc	0.02	0.01	0.03	0.02	0.01	0.03
Cwa	4.27	12.90	0.08	1.61	4.80	0.06
Cwb	0.77	2.34	0.00	0.26	0.79	0.00
Cwc	0.05	0.16	0.00	0.00	−0.01	0.00
Dfa	3.14	9.51	0.05	0.85	2.55	0.02
Dfb	1.27	3.45	0.21	−0.51	−1.64	0.04
Dfc	3.62	10.04	0.50	−0.16	−0.86	0.17
Dfd	0.25	0.77	0.00	0.24	0.73	0.00
Dsa	0.06	0.17	0.01	0.01	0.02	0.01
Dsb	0.06	0.18	0.00	0.01	0.03	0.00
Dsc	0.04	0.13	0.00	0.03	0.10	0.00
Dsd	0.00	0.00	0.00	0.00	0.00	0.00
Dwa	0.74	2.25	0.01	0.21	0.63	0.00
Dwb	0.22	0.66	0.00	−0.07	−0.21	0.00
Dwc	0.38	1.17	0.00	0.06	0.20	0.00
Dwd	0.00	0.00	0.00	0.00	0.00	0.00
ET	7.29	6.23	7.81	0.47	0.75	0.34
EF	8.16	10.11	7.21	0.42	−0.23	0.73

especially in precipitation, and this would be expected to impact the resultant K-G climatic types. In light of these considerations, the extent of correspondence confirms that the procedure is valid and that the CCSM4 generally provides reasonable simulations of the terrestrial, marine, and global K-G climate types.

4.2. Mid-Holocene (MH)

Fig. 2 maps the K-G climate types in the MH. Table 3 quantifies the percentage of Earth's surface covered by each climate type with a

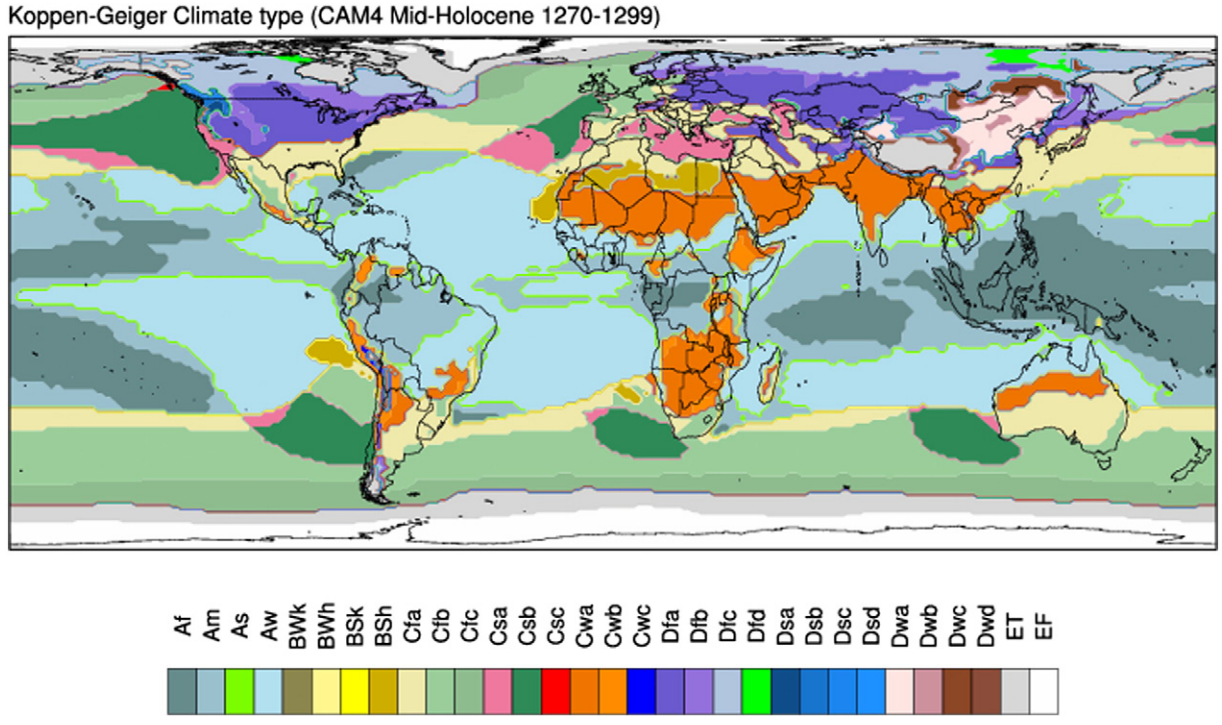

Fig. 2. K-G global climatic types at the mid-Holocene (6 ka) based on CMIP5 CCSM4-simulated values of monthly temperature and precipitation for 30 years.

comparison to the area covered in the 1976–2005 period. Comparison of Tables 1 and 3 suggests that the top four most extensive climates globally according to the CCSM4 simulation remained in the same order of areal extent from the MH to the 1976–2005 period. For terrestrial areas only, Table 3 suggests that the subtropical winter–dry, hot summer (Cwa) – a common monsoonal climate – appears to have been more extensive in the MH than in recent times, while Aw was slightly smaller in the MH than in recent years. For marine areas only, Table 3 suggests remarkably similar areal extents between the MH and the 1976 period, for all climate types.

Fig. 3a (b) shows the locations of MH (modern) K-G types that differ from the modern (MH). The largest continuous areas of changes occurred in North Africa, where BSh in the MH (Fig. 3a) migrated southward and was replaced by BWh by the 1976–2005 period (Fig. 3b), and in the equatorial Indian Ocean, where a large area west of Sumatra

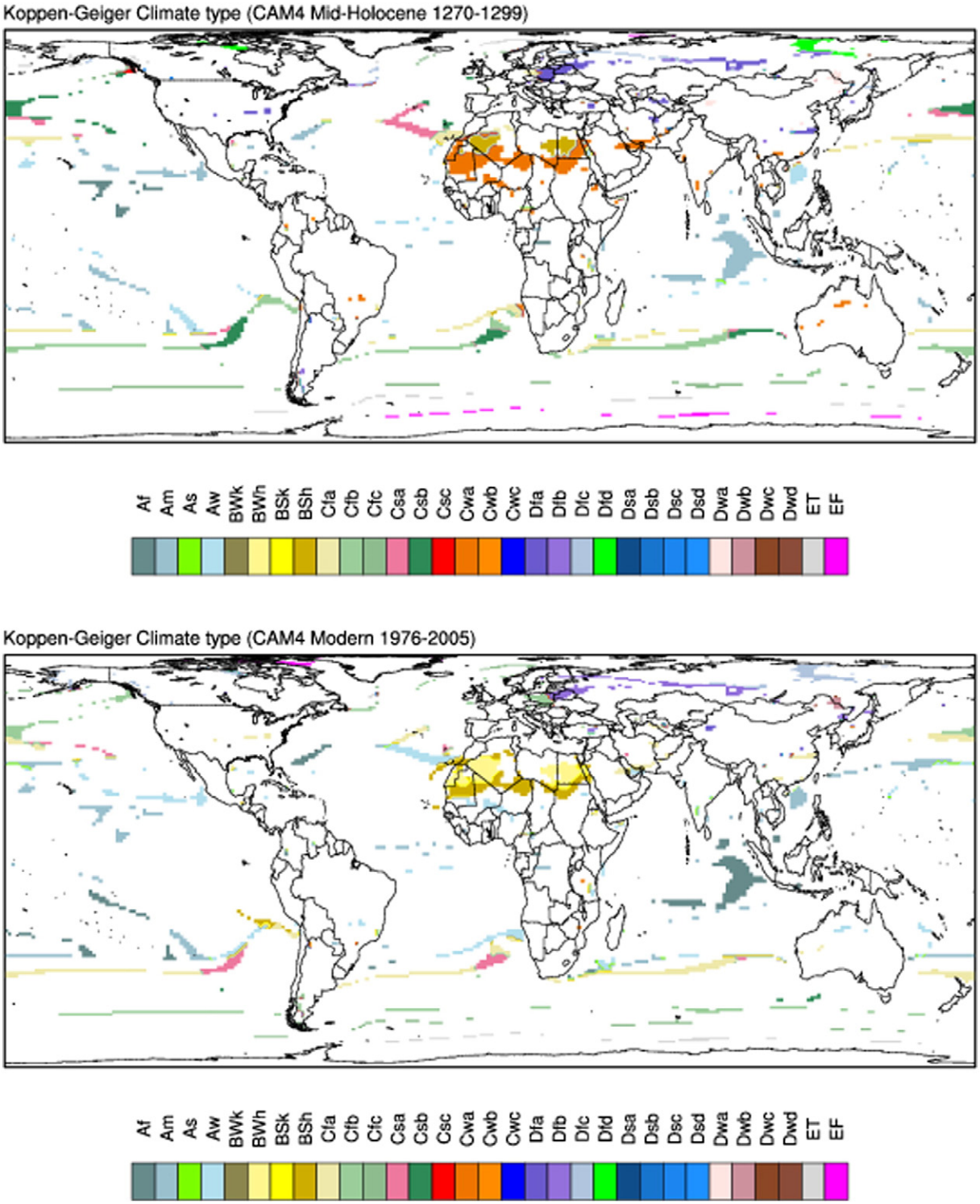

Fig. 3. Locations where K-G climatic type shifted from MH to modern (1976–2005) period. a) MH K-G climate; b) modern K-G climate.

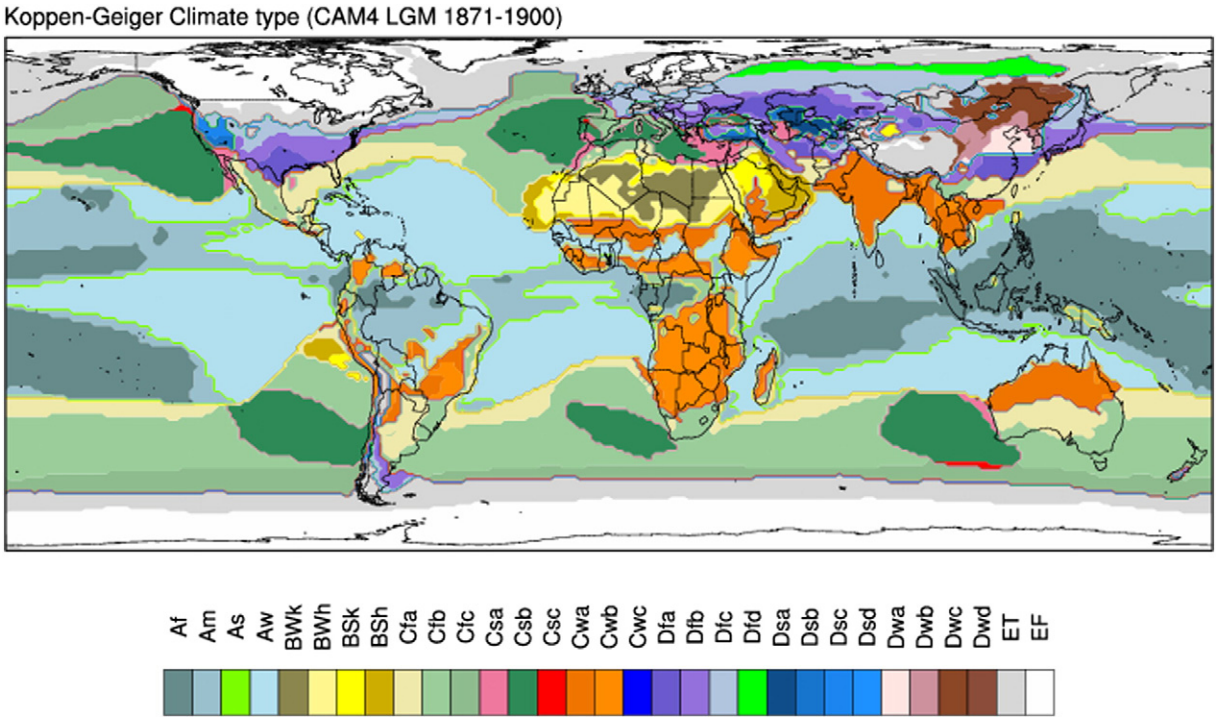

Fig. 4. As in Fig. 2, but for the Last Glacial Maximum (21 ka).

that had been an Am climate in the MH (Fig. 3a) changed to Af by the modern period (Fig. 3b). Smaller areas of the north Pacific Ocean also changed in climate type, mostly from Mediterranean (Cs_) in the MH to mesothermal humid (Cf_) in modern times.

4.3. Last Glacial Maximum (LGM)

Fig. 4 shows the geographic distribution of K-G climate types at the LGM. Our results correspond remarkably closely to the early study by

Table 4
CMIP5-simulated percentage of earth's surface area covered by each K-G climatic type: last glacial maximum, with comparison to modern (1976–2005) and mid-holocene.

	Percentage of Global Surface Area During LGM			CMIP5 LGM – MH			CMIP5: LGM – Modern		
	Total	Terrestrial	Marine	Total	Terrestrial	Marine	Total	Terrestrial	Marine
Af	7.98	3.39	10.72	−0.44	−0.26	−0.02	−1.63	−0.58	−1.63
Am	9.15	5.45	11.36	−2.83	−2.62	−2.52	−3.03	−2.79	−2.73
As	0.00	0.00	0.00	0.00	0.00	0.00	0.00	0.00	0.00
Aw	15.34	7.36	20.10	−3.33	−2.25	−2.97	−4.60	−4.85	−3.60
BSh	0.81	1.43	0.44	0.06	0.19	−0.07	−0.54	−1.22	−0.28
BSk	0.42	0.97	0.09	0.42	0.96	0.09	0.42	0.97	0.09
BWh	0.77	1.85	0.12	0.77	1.85	0.12	0.36	0.63	0.11
BWk	0.62	1.66	0.00	0.62	1.66	0.00	0.62	1.66	0.00
Cfa	4.91	4.62	5.07	−2.89	−6.35	−1.17	−3.55	−7.70	−1.51
Cfb	12.09	6.11	15.65	1.34	1.84	1.76	1.29	1.66	1.77
Cfc	4.32	0.34	6.69	−0.91	0.09	−0.95	−0.74	0.02	−0.67
Csa	0.52	1.06	0.20	−1.16	−0.25	−1.66	−1.20	−0.55	−1.58
Csb	5.84	0.95	8.76	1.47	0.44	2.51	2.28	0.38	3.74
Csc	0.12	0.07	0.16	0.10	0.06	0.13	0.12	0.07	0.16
Cwa	3.06	7.97	0.13	−1.22	−4.93	0.04	0.39	−0.14	0.11
Cwb	2.16	5.78	0.00	1.40	3.43	0.00	1.65	4.22	0.00
Cwc	0.04	0.12	0.00	−0.01	−0.04	0.00	−0.01	−0.05	0.00
Dfa	0.90	2.39	0.00	−2.24	−7.12	−0.04	−1.40	−4.57	−0.02
Dfb	1.65	3.93	0.29	0.38	0.48	0.07	−0.13	−1.16	0.11
Dfc	2.42	5.79	0.40	−1.20	−4.24	−0.10	−1.37	−5.10	0.07
Dfd	0.60	1.62	0.00	0.35	0.85	0.00	0.59	1.57	0.00
Dsa	0.23	0.60	0.00	0.16	0.43	−0.01	0.18	0.45	0.00
Dsb	0.16	0.39	0.02	0.10	0.21	0.02	0.11	0.25	0.02
Dsc	0.11	0.28	0.00	0.06	0.15	0.00	0.09	0.24	0.00
Dsd	0.00	0.00	0.00	0.00	0.00	0.00	0.00	0.00	0.00
Dwa	0.18	0.47	0.00	−0.57	−1.78	−0.01	−0.36	−1.15	−0.01
Dwb	0.27	0.73	0.00	−0.01	−0.14	0.00	0.06	0.07	0.00
Dwc	0.65	1.74	0.00	0.27	0.58	0.00	0.33	0.77	0.00
Dwd	0.07	0.18	0.00	0.07	0.18	0.00	0.07	0.18	0.00
ET	9.27	10.41	8.59	1.98	4.18	0.78	2.45	4.93	1.12
EF	15.35	22.33	11.19	7.20	12.21	3.99	7.61	11.98	4.72

Guetter and Kutzbach (1990); see their Fig. 1), though the coarser resolution in that study makes comparisons difficult. Table 4 quantifies the areal extent of the types, with areal differences from the LGM to the MH and from the LGM to the modern period. Table 4 shows that EF (Aw) was the most dominant terrestrial (marine) type at the LGM, and that the climate types that expanded most from the LGM to the MH were the Aw (globally and in marine areas) and humid continental - hot summer (Dfa) in terrestrial areas. Likewise the largest increases from the LGM to the modern period were again for Aw (globally and in marine areas) and Cfa over the terrestrial Earth (Table 4). Not surprisingly, the largest areal decreases from both the LGM to MH and from the LGM to modern period was EF, for global, terrestrial, and marine climates. ET showed the second-largest areal decrease for both the global and terrestrial areas, with the second-most-prominent oceanic decreases for Mediterranean—warm summer (Csb) across both subperiods. Arid and semi-arid (B) climates remained remarkably similar in

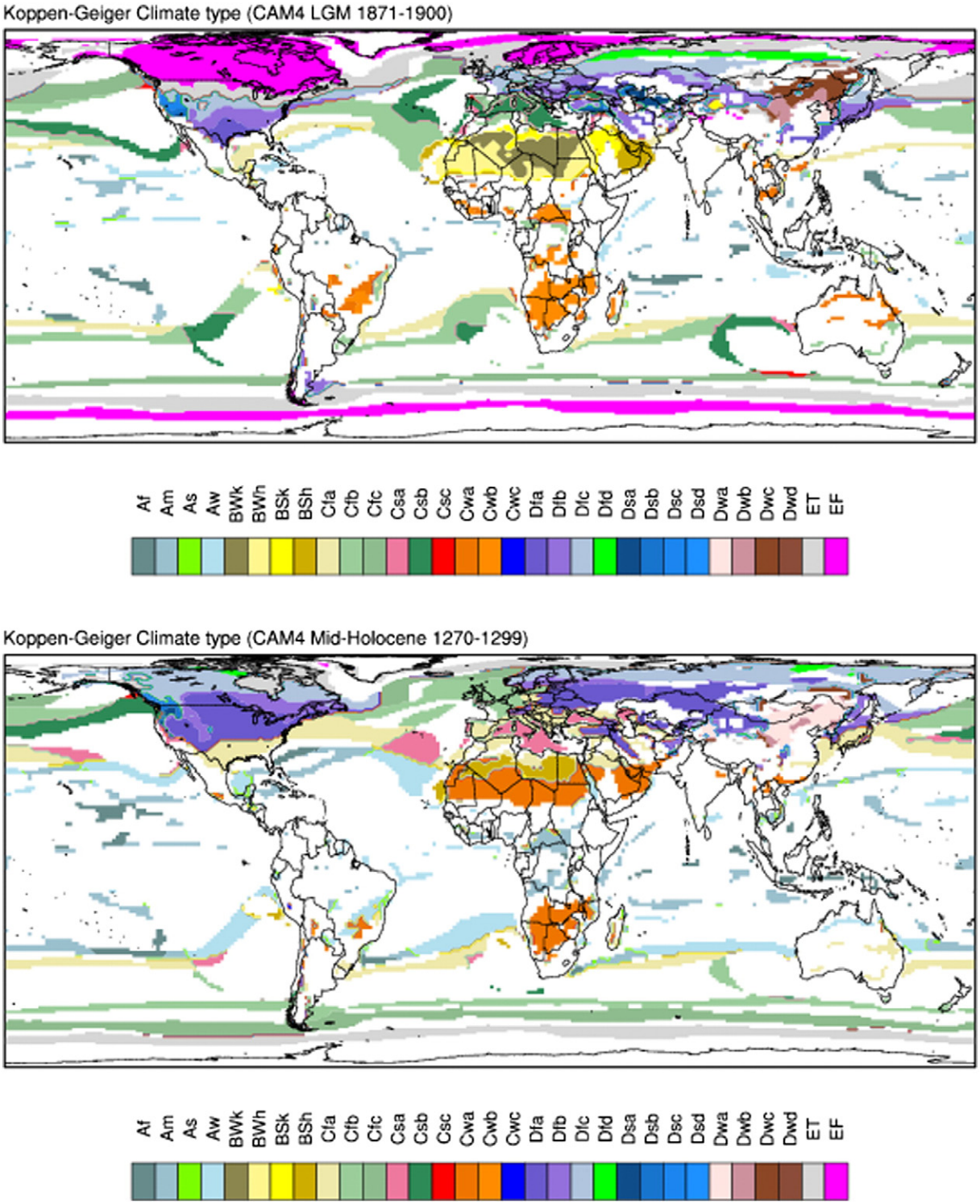

Fig. 5. Locations where K-G climatic type shifted from LGM to MH. a) LGM K-G climate; b) MH K-G climate.

total areal extent across the three periods, while mesothermal warm summer climates (C_b) of the LGM gave way to hot summer mid-latitude climates (C_a) over time for global, terrestrial, and marine areas.

Fig. 5a (b) shows the locations of LGM (MH) K-G types that differ from the MH (LGM), and Fig. 6a (b) shows the locations of LGM (modern) K-G types that differ from the modern (LGM). Most of the extratropical Earth, over both land and ocean, especially in the northern hemisphere, experienced climatic shifts from the LGM to the MH. Only slightly larger areas experienced climatic shifts from the LGM to the modern area, suggesting that the MH was similar climatologically to the modern era. Shifts over the equatorial Pacific Ocean call into question potential changing impacts to and by the Southern Oscillation phenomenon. Because Köppen-type classifications overlap closely with the biome distributions (Rohli et al., 2015b), these results may be helpful in identifying biotic realms from the geologic past and the potential vegetative response to future climate changes, particularly in light of concerns that the pace of shifts in climate zones may increase in a warming world (Mahlstein et al., 2013).

To assess the extent to which temperature and precipitation are driving the changes to K-G climatic types, Fig. 7a–f depicts the annual

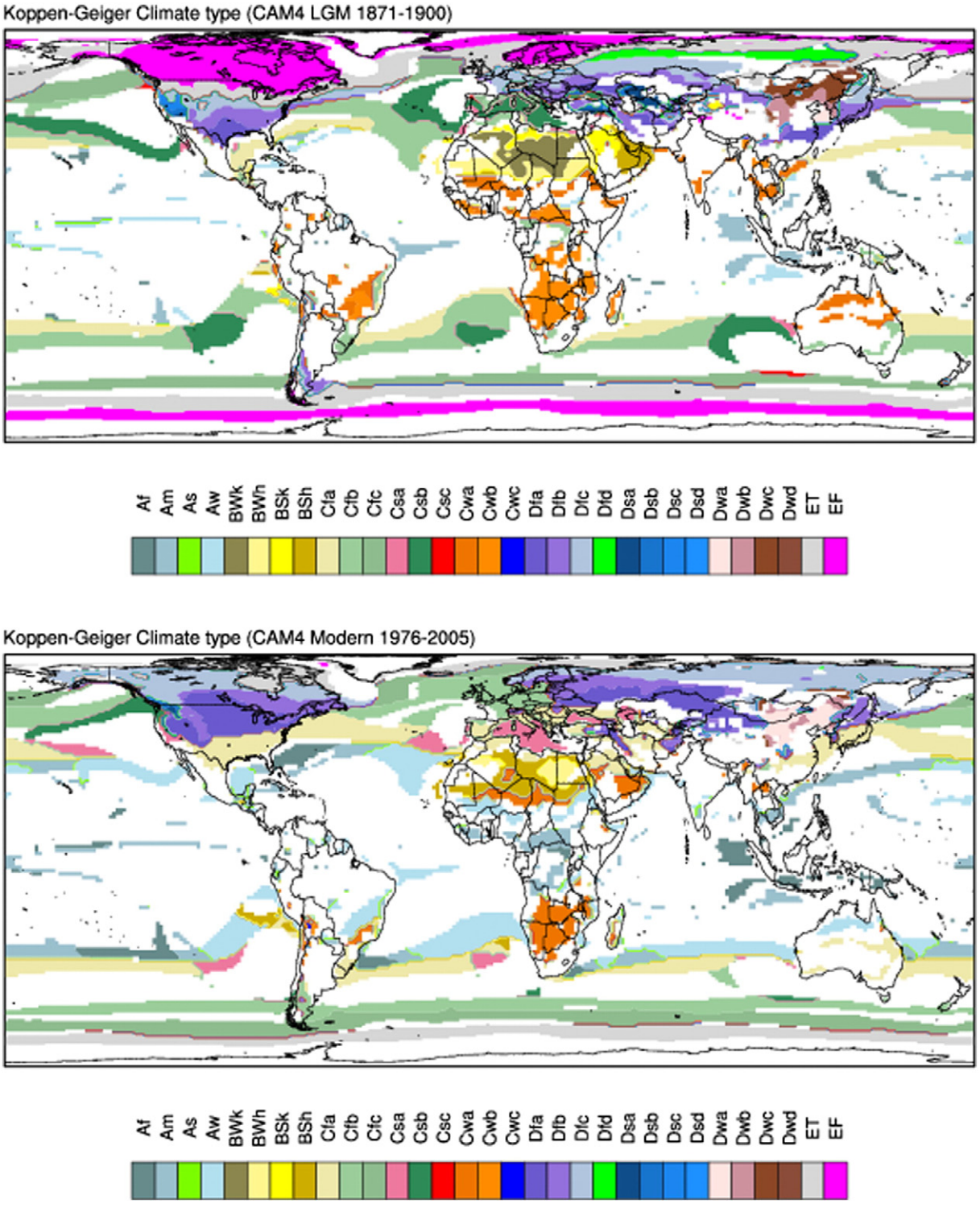

Fig. 6. Locations where K-G climatic type shifted from LGM to modern (1976–2005) period. a) LGM K-G climate; b) modern K-G climate.

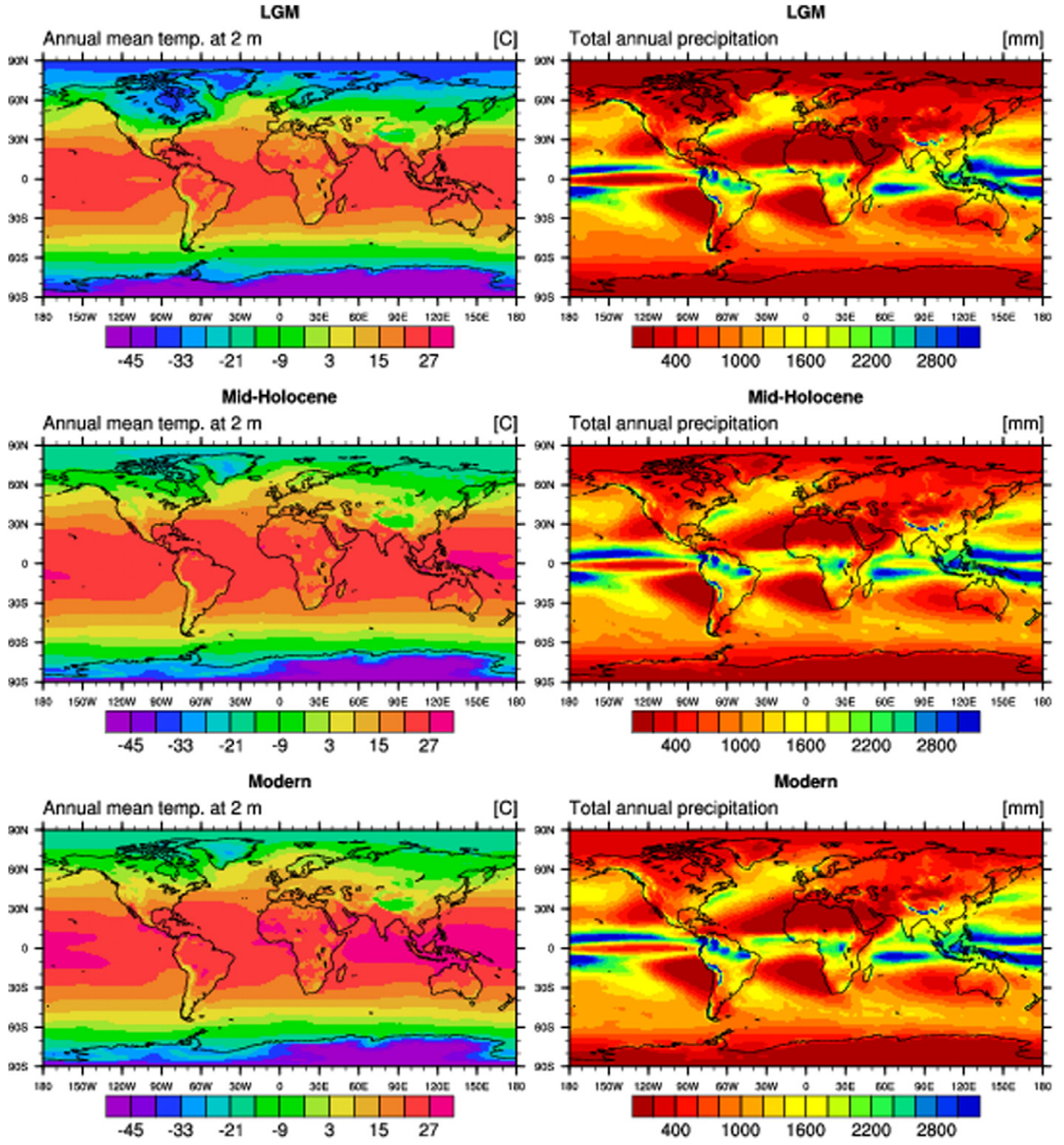

Fig. 7. Annual mean temperature and total precipitation in LGM, MH, and modern period, respectively.

mean temperature and total precipitation in the LGM, MH, and 1976–2005 period, respectively. Although temperature and/or precipitation changes that do not produce a change in K-G climate type are of little practical significance because they would theoretically produce no change in biomes, small numerical differences in temperature or precipitation totals and/or seasonality could result in shifts in major bioclimatic realms if they cause a change in K-G climate types.

Not surprisingly, the reduced temperatures of the LGM appear playing a major role globally, including the tropics (compare Fig. 7a–c and e). However, decreased precipitation during the LGM, as compared to the MH and modern period (compare Fig. 7b–d and f), seems to be another factor contributing to the relative consistency in tropical and (especially) subtropical climate types, particularly in arid areas. As such climates warmed, they also became wetter, often offsetting the tendency for desertification.

5. Conclusions

This research has shown the changing areal extent and geography of the Köppen–Geiger (K-G) climate types over the last 21,000 years using

the CCSM4 simulation results as part of the PMIP3/CMIP5. However, this study is limited in a few ways. First, CCSM4 model outputs are available only for a few decades for the LGM and MH periods, which might not fully represent the prehistoric climate conditions during the periods. Also, while the paleoclimate proxy data were incorporated in the CCSM4 simulations, they cannot be free of defects. In particular, there are many uncertainties existing in GCM simulations with boundary conditions and the initial state of paleoclimates as well as model variability. Therefore, caution should be used in interpreting the results of paleoclimate simulations and their manifestations in the K-G climate types.

Since the LGM, the extent and position of the ice cap and tundra climates have undergone the most extensive shifts and decreases in areal extent, and in general, climates of the northern hemisphere have shifted more noticeably than those in the southern hemisphere. Hot summer mesothermal and microthermal climates exhibited large increases in area, while over marine areas, tropical wet–dry expanded more than any other climate. Future research should be conducted to overlay the atmospheric circulation changes as simulated by CCSM4 CAM4 and changes in ocean currents as simulated by CCSM4 POP2 ocean model with our modeled changes in climatic types.

Acknowledgments

The authors appreciate the support of Dr. Joseph Galewsky and the University of New Mexico.

References

Baker, B., Diaz, H., Hargrove, W., Hoffman, F., 2010. Use of the Köppen–Trewartha climate classification to evaluate climatic refugia in statistically derived ecoregions for the People's Republic of China. Clim. Chang. 98, 113–131.
Beck, C., Grieser, J., Kottek, M., Rubel, F., Rudolf, B., 2006. Characterizing global climate change by means of Köppen climate classification. In: German Weather Service (Ed.), Klimastatusbericht 2005, pp. 139–149.
Belda, M., Holtanová, E., Halenka, T., Kalvová, J., 2014. Climate classification revisited: from Köppen to Trewartha. Clim. Res. 59, 1–13.
Berg, A., de Noblet-Ducoudre, N., Sultan, B., Lengaigne, M., Guimberteau, M., 2013. Projections of climate change impacts on potential C_4 crop productivity over tropical regions. Agric. For. Meteorol. 170, 89–102.
Born, K., Fink, A.H., Paeth, H., 2008. Dry and wet periods in the northwestern Maghreb for present day and future climate conditions. Meteorol. Z. 17, 533–551.
Braconnot, P., Harrison, S., Kageyama, M., Bartlein, P.J., Masson-Delmotte, V., Abe-Ouchi, A., Otto-Bliesner, Zhao, Y., 2012. Evaluation of climate models using paleoclimatic data. Nat. Clim. Chang. 2, 417–424.
Braconnot, P., Otto-Bliesner, B., Harrison, S., Joussaume, S., Peterchmitt, J.-Y., Abe-Ouchi, A., Crucifix, M., Driesschaert, E., Fichefet, T., Hewitt, C.D., Kageyama, M., Kitoh, A., Laîné, A., Loutre, M.-F., Marti, O., Merkel, U., Ramstein, G., Valdes, P., Weber, S.L., Yu, Y., Zhao, Y., 2007. Results of PMIP2 coupled simulations of the Mid-Holocene and Last Glacial Maximum – Part 1: Experiments and large-scale features. Clim. Past 3, 261–277.
Brady, E.C., Otto-Bliesner, B.L., Kay, J.E., Rosenbloom, N., 2013. Sensitivity to glacial forcing in the CCSM4. J. Clim. 26, 1901–1925.
Briegleb, B.P., Bitz, C.M., Hunke, E.C., Lipscomb, W.H., Holland, M.M., Schramm, J.L., Moritz, R.E., 2004. Scientific description of the sea ice component in the Community Climate System Model, Version 3. NCAR Tech. Note NCAR/TN-463 + STR (70 pp.).
Broccoli, A.J., 2000. Tropical cooling at the Last Glacial Maximum: an atmosphere–mixed layer ocean model simulation. J. Clim. 13, 951–976.
Chen, D., Chen, H.W., 2013. Using the Köppen classification to quantify climate variation and change: an example for 1901–2010. Environ. Dev. 6, 69–79.
Cohen, J., 1960. A coefficient of agreement for nominal scales. Educ. Psychol. Meas. 20, 37–46.
Crosbie, R.S., Pollock, D.W., Mpelasoka, F.S., Barron, O.V., Charles, S.P., Donn, M.J., 2012. Changes in Köppen–Geiger climate types under a future climate for Australia: hydrological implications. Hydrol. Earth Syst. Sci. 16, 3341–3349.
Crucifix, M., Betts, R.A., Hewitt, C.D., 2005. Pre-industrial-potential and Last Glacial Maximum global vegetation simulated with a coupled climate-bio sphere model: diagnosis of bioclimatic relationships. Glob. Planet. Chang. 45, 295–312.
Dantas, A.A.A., de Carvalho, L.G., Ferreira, E., 2007. Climatic classification and tendencies in Lavras region MG. Cienc. Agrotecnol. 31, 1862–1866.
Denk, T., Grimm, G.W., Grimsson, F., Zetter, R., 2013. Evidence from "Köppen signatures" of fossil plant assemblages for effective heat transport of Gulf Stream to subarctic North Atlantic during Miocene cooling. Biogeosciences 10, 7927–7942.
Diaz, H.F., Eischeid, J.K., 2007. Disappearing "alpine tundra" Köppen climatic type in the western United States. Geophys. Res. Lett. 34, L18707.
Elguindi, N., Grundstein, A., Bernardes, S., Turuncoglu, U., Feddema, J., 2014. Assessment of CMIP5 global model simulations and climate change projections for the 21(st) century using a modified Thornthwaite climate classification. Clim. Chang. 122, 523–538.
Feddema, J.J., 2005. A revised Thornthwaite-type global climate classification. Phys. Geogr. 26, 442–466.
Feng, S., Ho, C.-H., Hu, Q., Oglesby, R.J., Jeong, S.J., Kim, B.M., 2011. Evaluating observed and projected future climate changes for the Arctic using the Köppen–Trewartha climate classification. Clim. Dyn. 38, 1359–1373.
Feng, S., Hu, Q., Huang, W., Ho, C.H., Li, R.P., Tang, Z.H., 2014. Projected climate regime shift under future global warming from multi-model, multi-scenario CMIP5 simulations. Glob. Planet. Chang. 112, 41–52.
Forgy, E.W., 1965. Cluster analysis of multivariate data: efficiency versus interpretability of classifications. Biometrics 21, 768–769.
Fraedrich, K., Gerstengarbe, F.W., Werner, P.C., 2001. Climate shifts during the last century. Clim. Chang. 50, 405–417.
Gallardo, C., Gil, V., Hagel, E., Tejeda, C., de Castro, M., 2013. Assessment of climate change in Europe from an ensemble of regional climate models by the use of Köppen–Trewartha classification. Int. J. Climatol. 33, 2157–2166.
Geiger, R., 1961. Überarbeitete Neuausgabe von Geiger, R.: Köppen-Geiger/Klima der Erde. (Wandkarte 1:16 Mill.) (Revised reissue of Geiger, R.: Köppen-Geiger/Climate of the Earth. (Wall map 1:16 Mill.)) – Klett-Perthes, Gotha.
Gent, P.R., Danabasoglu, G., Donner, L.J., Holland, M.M., Hunke, E.C., Jayne, S.R., Lawrence, D.M., Neale, R.B., Rasch, P.J., Vertenstein, M., Worley, P.H., Yang, Z.-L., Zhang, M., 2011. The Community Climate System Model version 4. J. Clim. 24, 4973–4991.
Guetter, P.J., Kutzbach, J.E., 1990. A modified Köppen classification applied to model simulations of glacial and interglacial climates. Clim. Chang. 16, 193–215.
Hanf, F., Körper, J., Spangehl, T., Cubasch, U., 2012. Shifts of climate zones in multi-model climate change experiments using the Köppen climate classification. Meteorol. Z. 21, 111–123.
Harrison, S.P., Bartlein, P.J., Brewer, S., Prentice, I.C., Boyd, M., Hessler, I., Holmgren, K., Izumi, K., Willis, K., 2014. Climate model benchmarking with glacial and mid-Holocene climates. Clim. Dyn. 43, 671–688.
Holdridge, L.R., 1947. Determination of world plant formations from simple climatic data. Science 105, 367–368.
Jacob, D., Elizalde, A., Haensler, A., Hagemann, S., Kumar, P., Podzun, R., Rechid, D., Remedio, A.R., Saeed, F., Sieck, K., Teichmann, C., Wilhelm, C., 2012. Assessing the transferability of the regional climate model REMO to different coordinated regional climate downscaling experiment (CORDEX) regions. Atmosphere 3, 181–199.
Jylhä, K., Tuomenvirta, H., Ruosteenoja, K., Hiemi-Hugaerts, H., Keisu, K., Karhu, J.A., 2010. Observed and projected future shifts of climatic zones in Europe and their use to visualize climate change information. Weather Clim. Soc. 2, 148–167.
Kalnay, E., Kanamitsu, M., Kistler, R., Collins, W., Deaven, D., Gandin, L., et al., 1996. The NCEP/NCAR 40-year reanalysis project. B. Am. Meteorol. Soc. 77, 437–471.
Kalvová, J., Halenka, T., Bezpalcová, K., Nemešová, I., 2003. Köppen climate types in observed and simulated climates. Stud. Geophys. Geod. 47, 185–202.
Kim, H.-J., Wang, B., Ding, Q., Chung, I.-U., 2008. Changes in arid climate over north China detected by the Köppen climate classification. J. Meteorol. Soc. Jpn. 86, 981–990.
Köppen, W., 1884. The thermal zones of the Earth. Meteorol. Z. 39.
Köppen, W., 1936. Das geographische System der Klimate. In: Köppen, W., Geiger, R. (Eds.), Handbuck der Klimatologie Bd. 1, Teil C.Gebrüder Bornträger, Berlin
Köppen, W., 2011. (translated and edited version). The thermal zones of the Earth according to the duration of hot, moderate and cold periods and to the impact of heat on the organic world. Meteorol. Z. 20, 351–360.
Korty, R.L., Camargo, S.J., Galewsky, J., 2012a. Tropical cyclone genesis factors in simulations of the Last Glacial Maximum. J. Clim. 25, 4348–4365.
Korty, R.L., Camargo, S.J., Galewsky, J., 2012b. Variations in tropical cyclone genesis factors in simulations of the Holocene Epoch. J. Clim. 25, 8196–8211.
Kottek, M., Grieser, J., Beck, C., Rudolf, B., Rubel, F., 2006. World map of the Köppen–Geiger climate classification updated. Meteorol. Z. 15, 259–263.
Kutzbach, J.E., 1988. Major climatic changes of the last 18,000 years: observations and model simulations. Science 241 (4869), 1043–1052.
Lawrence, D.M., Oleson, K.W., Flanner, M.G., Fletcher, C.G., Lawrence, P.J., Levis, S., Swenson, S.C., Bonan, G.B., 2012. The CCSM4 land simulation, 1850–2005: assessment of surface climate and new capabilities. J. Clim. 25, 2240–2260.
Lawrence, P.J., Chase, T.N., 2007. Representing a new MODIS consistent land surface in the Community Land Model (CLM3.0). J. Geophys. Res. 112, G01023.
Mahlstein, I., Daniel, J.S., Solomon, S., 2013. Pace of shifts in climate regions increases with global temperature. Nat. Clim. Chang. 3, 739–743.
Mitchell, M., Kienholz, J., 1997. A climatological analysis of the Köppen Dfa/Dfb boundary in eastern North America, 1901–1990. Ohio J. Sci. 97, 53–58.
Monserud, R.A., Leemans, R., 1992. Comparing global vegetation maps with the kappa-statistic. Ecol. Model. 62, 275–293.
Neale, R.B., Richter, J., Park, S., Lauritzen, P.H., Vavrus, S.J., Rasch, P.J., Zhang, M., 2013. The mean climate of the Community Atmosphere Model (CAM4) in forced SST and fully coupled experiments. J. Clim. 26, 5150–5168.
Otto-Bliesner, B.L., Brady, E.C., Clauzet, G., Tomas, R., Levis, S., Kothavala, Z., 2006. Last Glacial Maximum and Holocene climate in CCSM3. J. Clim. 19, 2526–2544.
Park, C.-Y., Choi, Y., Kwon, Y.-A., Kwon, J.-I., Lee, H.-S., 2013. Studies on changes and future projections of subtropical climate zones and extreme temperature events over South Korea using high resolution climate change scenario based on PRIDE model. J. Korean Assoc. Reg. Geogr. 19, 600–614.
Peel, M.C., Finlayson, B.L., McMahon, T.A., 2007. Updated world map of the Köppen–Geiger climate classification. Hydrol. Earth Syst. Sci. 11, 1633–1644.
Rahimi, J., Ebrahimpour, M., Khalili, A., 2013. Spatial changes of Extended De Martonne climatic zones affected by climate change in Iran. Theor. Appl. Climatol. 112, 409–418.

Roderfeld, H., Blyth, E., Dankers, R., Huse, G., Slagstad, D., Ellingsen, I., Wolf, A., Lange, M.A., 2008. Potential impact of climate change on ecosystems of the Barents Sea region. Clim. Chang. 87, 283–303.
Rohli, R.V., Joyner, T.A., Reynolds, S.J., Shaw, C., Vázquez, J.R., 2015a. Globally extended Köppen–Geiger climate classification and temporal shifts in terrestrial climatic types. Phys. Geogr. 36, 142–157.
Rohli, R.V., Joyner, T.A., Reynolds, S.J., Ballinger, T.J., 2015b. Overlap of global Köppen–Geiger climates, biomes, and soil orders. Phys. Geogr. 36, 158–175.
Rubel, F., Kottek, M., 2010. Observed and projected climate shifts 1901–2100 depicted by world maps of the Köppen–Geiger climate classification. Meteorol. Z. 19, 135–141.
Shin, S.-H., Bae, D.-H., 2013. Future projections of Köppen climate shifts in the Asia regions using A2 scenario. J. Korea Water Resour. Assoc. 46, 253–265.
Shin, S.-H., Chung, I.-U., Kim, H.-J., 2012. Relationship between the expansion of drylands and the intensification of Hadley circulation during the late twentieth century. Meteorog. Atmos. Phys. 118, 117–128.
Suckling, P.W., Mitchell, M.D., 2000. Variation of the Köppen C/D climate boundary in the central United States during the 20th century. Phys. Geogr. 21, 38–45.
Teichmann, C., Eggert, B., Elizalde, A., Haensler, A., Jacob, D., Kumar, P., Moseley, C., Pfeifer, S., Rechid, D., Remdeio, A.R., Ries, H., Petersen, J., Preuschmann, S., Raub, T., Saeed, F., Sieck, K., Weber, T., 2013. How does a regional climate model modify the projected climate change signal of the driving GCM: a study over different CORDEX regions using REMO. Atmosphere 4, 214–236.
Thornthwaite, C.W., 1948. An approach toward a rational classification of climate. Geogr. Rev. 33, 233–255.
Thornton, P.E., Lamarque, J.F., Rosenbloom, N.A., Mahowald, N.M., 2007. Influence of carbon/nitrogen cycle coupling on land model response to CO_2 fertilization and climate variability. Glob. Biogeochem. Cycles 21, GB4018.
Trewartha, G.T., 1968. An Introduction to Climate. McGraw-Hill, New York, NY.
Wang, M.Y., Overland, J.E., 2004. Detecting Arctic climate change using Köppen climate classification. Clim. Chang. 67, 43–62.
Wong, S.L., Wan, K.W., Yang, L., Lam, J.C., 2012. Changes in bioclimates in different climates around the world and implications for the built environment. Build. Environ. 57, 214–222.
Yun, K.-S., Heo, K.-Y., Chu, J.-E., Ha, K.-J., Lee, E.-J., Choi, Y., Kitoh, A., 2012. Changes in climate classification and extreme climate indices from a high-resolution future projection in Korea. Asia-Pac. J. Atmos. Sci. 48, 213–226.
Zhang, X., Yan, X., 2014. Spatiotemporal change in geographical distribution of global climate types in the context of climate warming. Clim. Dyn. 43, 595–605.
Zhang, Z., Flatøy, F., Wang, H., Bethke, I., Bentsen, M., Guo, Z., 2012. Early Eocene Asian climate dominated by desert and steppe with limited monsoons. J. Asian Earth Sci. 44, 24–35.